

# Compensation Topologies of High-Power Wireless Power Transfer Systems

Wei Zhang, *Student Member, IEEE*, and Chunting Chris Mi, *Fellow, IEEE*

**Abstract**—Wireless power transfer (WPT) is an emerging technology that can realize electric power transmission over certain distances without physical contact, offering significant benefits to modern automation systems, medical applications, consumer electronics, etc. This paper provides a comprehensive review of existing compensation topologies for the loosely coupled transformer. Compensation topologies are reviewed and evaluated based on their basic and advanced functions. Individual passive resonant networks used to achieve constant (load-independent) voltage or current output are analyzed and summarized. Popular WPT compensation topologies are given as application examples, which can be regarded as the combination of multiple blocks of resonant networks. Analyses of the input zero phase angle and soft switching are conducted as well. This paper also discusses the compensation requirements for achieving the maximum efficiency according to different WPT application areas.

**Index Terms**—Compensation topology, efficiency, input zero phase angle (ZPA), load-independent voltage and current output, soft switching, wireless power transfer (WPT) system.

## I. INTRODUCTION

ENGINEERS have dreamt of delivering electrical power wirelessly over the air for more than a century. Wireless or inductive power transfer was first suggested soon after the proposition of Faraday's law of induction, which is the underpinning of modern wireless power transfer (WPT), as well as electrical engineering. In the 1910s, Nikola Tesla, who is the pioneer of WPT technology, put forward his aggressive ideas of using his Wardencllyffe Tower for wirelessly transmitting useful amounts of electrical power around the world [1], [2]. Although his strategy for accomplishing this desire was impractical and ultimately unsuccessful, his contribution to wireless energy transmission has never faded [3], [4].

Nowadays, WPT has grown to a \$1 billion commercial industry around the world [5]. This technology has found applications in charging home appliances such as electric toothbrushes, wireless charging of mobile phones using a charging platform [6]–[13], and medical uses such as wireless power supply to implantable devices [14]–[20]. Medium- to high-

power applications of this technology include continuous power transfer to people movers [21], [22] and contactless battery charging for a moving actuator [23], [24] or electric vehicles (EVs) [25]–[36].

To transfer power without physical contact, a loosely coupled transformer that involves a large separation between the primary and secondary windings is essential. Due to the large winding separation, it has a relatively large leakage inductance, as well as increased proximity effect and winding resistances. Furthermore, the magnetizing flux is significantly reduced, which results in a much lower magnetizing inductance and mutual inductance.

For coils of a WPT system operating at a frequency well below their self-resonant frequencies [37], additional compensation capacitors are needed to form the resonant tanks in both the primary and secondary sides. Single-sided compensation appears in some previous wireless circuit designs [19], [38]. It has been replaced by double-sided compensation since single-sided compensation has fewer adjustable resonant parameters, which cannot provide enough degrees of freedom to satisfy all WPT system design criteria. This paper reviews, compares, and evaluates compensation topologies for WPT systems and its applications.

## II. REQUIREMENT FOR COMPENSATION

1) *Minimized VA Rating and Maximized Power Transfer Capability*: The basic requirement for a compensation capacitor is to resonate with the primary and/or secondary inductance, to provide the reactive power required for the inductances to generate an adequate magnetic field [39]. Therefore, for the primary coil of the loosely coupled transformer, the basic function of compensation is to minimize the input apparent power or to minimize the volt-ampere (VA) rating of the power supply [28], [40], [41]. In the secondary side, compensation cancels the inductance of the secondary coil to maximize the transfer capability [29], [42], [43].

2) *Constant-Voltage or Current Output*: A WPT system has many parameters that may change during operation. For instance, the air gap changes in real time for a transcutaneous energy transmission system when the patient is breathing [20], [44]. The number of loads may change during charging for a roadway vehicle inductive power transfer (IPT) system [5], [25], [29]. Therefore, good controllability is desirable for a WPT system to cope with parameter variation. Meanwhile, the compensation topology can be selected to realize constant-current (or load-independent) or constant-voltage

Manuscript received January 27, 2015; revised April 22, 2015; accepted July 2, 2015. Date of publication July 8, 2015; date of current version June 16, 2016. This work was supported in part by the U.S. Department of Energy; The US-China Clean Energy Research Center—Clean Vehicle Consortium; and DENSO International. The review of this paper was coordinated by Mr. D. Diallo.

W. Zhang is with the University of Michigan, Dearborn, MI 48128 USA (e-mail: w.zhang112@gmail.com).

C. C. Mi is with the Department of Electrical and Computer Engineering, San Diego State University, San Diego, CA 92182 USA (e-mail: mi@ieee.org).

Color versions of one or more of the figures in this paper are available online at <http://ieeexplore.ieee.org>.

Digital Object Identifier 10.1109/TVT.2015.2454292

output without a control circuit, which is advantageous for achieving good controllability.

3) *High Efficiency*: According to the study in [45] and [46], the maximum achievable efficiency of a WPT system is only decided by two parameters, namely, the coupling coefficient and the quality factors of the windings. However, adequate compensation is necessary to achieve this maximum efficiency. High efficiency is also guaranteed by soft switching. A half-bridge or a full-bridge converter is commonly used for the modulation of a dc voltage to drive the resonant circuit. If metal–oxide–semiconductor field-effect transistors (MOSFETs) are used as switching components, the converter can benefit from turn-on zero-voltage switching by operating at above resonance, where the resonant-tank current is lagging the voltage modulated by the active switches [47]. Since this input phase angle can be adjusted by the value of compensation capacitors, the compensation should also be selected with consideration for soft switching.

4) *Bifurcation Resistant and Others*: The bifurcation phenomenon in a WPT system refers to the situation in which the frequency to realize a zero phase angle (ZPA) is not unique [40], [48]. The number of frequency points to realize a ZPA is related to the loading condition, compensation topologies, and capacitor values. This bifurcation phenomenon, which is accompanied with multiple loading and variable frequency control, should be avoided to guarantee system stability. Other features, such as insensitivity to parameter change and suitability for bidirectional power flow, should also be considered for special applications. Compensation topologies should be evaluated based on the aforementioned compensation purposes and by combining their applications and expected operations. The following sections discuss some of the primary features previously mentioned, along with several typical compensation topologies.

### III. CONSTANT-VOLTAGE OR CONSTANT-CURRENT OUTPUT PRINCIPLES

This section investigates how to achieve constant-current or constant-voltage output using resonant circuits. The constant-current or constant-voltage output realized by a resonant network refers to the voltage or current magnitude ( $U_{OUT}$  or  $I_{OUT}$ ) on loading resistance  $R_L$  that is irrelevant with the value of  $R_L$ ; hence, the resonant network has an output of voltage or current source characteristics.

In WPT resonant circuit analysis, the frequency-domain equivalent circuit is always assumed, and only the fundamental component is considered for simplicity [12], [28], [40], [49], [50]. The fundamental component approximation is a simple analysis method that can usually achieve sufficient accuracy for a high-quality factor resonant circuit that works near resonance; however, the switching components of an H-bridge inverter and rectifier will introduce some error. Then, if a more accurate study is conducted, such as investigating zero-current switching requirements (the accurate primary current when switching on), the higher-order harmonics should be considered [48]. In this paper, we use only the fundamental component to analyze the resonant network characteristics.

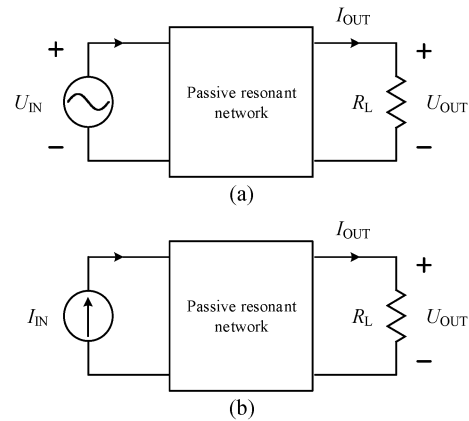


Fig. 1. Resonant circuit with (a) voltage source input and (b) current source input.

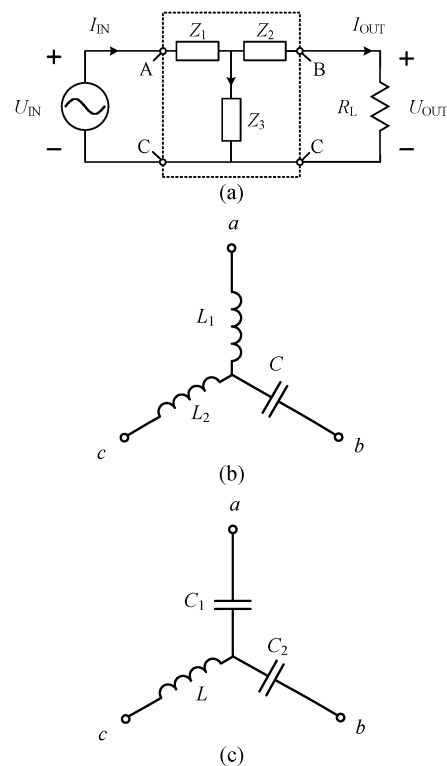


Fig. 2. Resonant network configuration with a (a) T-circuit model, (b) type A, and (c) type B to have constant-voltage output from a voltage source.

#### A. Constant-Voltage Output Principle

1) *Input Voltage Source*: The model of a passive resonant network is shown in Fig. 1. The power source can be a voltage source or a current source. To make the output voltage amplitude irrelevant with the value of  $R_L$ , the configuration of the passive resonant network must depend on the type of power source. If a voltage power source is used, the resonant network, to have a constant-voltage output, should have a T-circuit configuration, as shown in Fig. 2(a).

The T-circuit in Fig. 2(a) has the following equations:

$$\begin{aligned}
 U_{OUT} &= I_{OUT} \cdot R_L \\
 U_{IN} &= I_{IN} \cdot Z_1 + (I_{IN} - I_{OUT}) \cdot Z_3 \\
 U_{IN} &= I_{IN} \cdot Z_1 + I_{OUT} \cdot Z_2 + U_{OUT}.
 \end{aligned} \tag{1}$$

The relationship between input voltage  $U_{IN}$  and output voltage  $U_{OUT}$  can be derived as

$$U_{IN} = \left(1 + \frac{Z_1}{Z_3}\right) U_{OUT} + \frac{\Lambda}{R_L} \cdot U_{OUT} \quad (2)$$

where

$$\Lambda = \frac{Z_1 Z_2 + Z_2 Z_3 + Z_1 Z_3}{Z_3}. \quad (3)$$

In (2), if  $\Lambda = 0$ , the output voltage  $U_{OUT}$  is independent of  $R_L$ , and its output has the characteristics of a voltage source.

If circuit points A, B, and C in Fig. 2(a) are connected with circuit points a, b, and c in Fig. 2(b), respectively, then

$$\Lambda = \frac{L_1 + L_2 - \omega^2 L_1 L_2 C}{j\omega L_2 C}. \quad (4)$$

Moreover,  $\Lambda = 0$  requires the operating frequency of the resonant network at

$$\omega = \sqrt{\frac{1}{L_1 C} + \frac{1}{L_2 C}}. \quad (5)$$

It has a constant-voltage output

$$\frac{U_{OUT}}{U_{IN}} = \frac{L_2}{L_1 + L_2}. \quad (6)$$

If the circuit in Fig. 2(b) is rotated  $120^\circ$ , and we connect circuit points A, B, and C in Fig. 2(a) with circuit points c, b, and a, respectively, the circuit can also achieve a constant-voltage output of

$$\frac{U_{OUT}}{U_{IN}} = \frac{L_1}{L_1 + L_2} \quad (7)$$

at the operating frequency of (5).

We name the T-circuit topology in Fig. 2(b), which has two resonant inductors and one capacitor, as type A. Similarly, the type-B configuration with two resonant capacitors and one inductor in Fig. 2(c) can be also used as the constant-voltage output. The operating frequency is given without derivation, i.e.,

$$\omega = \frac{1}{\sqrt{LC_1 + LC_2}}. \quad (8)$$

Several typical compensation topologies can be summarized based on Fig. 2 for constant-voltage output from a voltage source. The configurations with numbers are listed in Table I.

Topologies V-V-7 and V-V-8 operate as two special cases. For V-V-7, if  $Z_3 = \infty$ , which is operating as an open circuit, the output voltage is equal to the input voltage when  $L$  and  $C$  resonate at the operating frequency. While for V-V-8, if  $Z_1 = Z_2 = 0$ , which is a short circuit, the output voltage is equal to the input voltage regardless of the value of  $Z_3$ .

2) *Input Current Source*: If the input is a current source as in Fig. 1(b), the resonant networks needed to realize a constant-voltage output should have the topologies shown in Fig. 3.

Output voltage  $U_{OUT}$  and input current  $I_{IN}$  of type-A topology in Fig. 3(a) can be represented by the following:

$$U_{OUT} = \frac{1}{j\omega C} i_{IN} - \left(j\omega L + \frac{1}{j\omega C}\right) i_{OUT}. \quad (9)$$

TABLE I  
SUMMARY OF CONSTANT-VOLTAGE OUTPUT FROM A VOLTAGE SOURCE

Number	Passive resonant network	Resonant frequency
V-V-1		$\omega = \sqrt{\frac{1}{L_1 C} + \frac{1}{L_2 C}}$
V-V-2		$\omega = \frac{1}{\sqrt{LC_1 + LC_2}}$
V-V-3		$\omega = \frac{1}{\sqrt{LC_1 + LC_2}}$
V-V-4		$\omega = \frac{1}{\sqrt{LC_1 + LC_2}}$
V-V-5		$\omega = \sqrt{\frac{1}{L_1 C} + \frac{1}{L_2 C}}$
V-V-6		$\omega = \sqrt{\frac{1}{L_1 C} + \frac{1}{L_2 C}}$
V-V-7		$\omega = \frac{1}{\sqrt{LC}}$
V-V-8		---

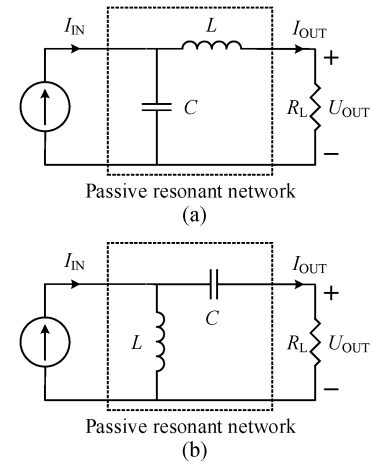


Fig. 3. Resonant circuits (a) type A and (b) type B to have constant-voltage output from a current source.

It is readily seen that the second term on the right-hand side of (9) can be eliminated if  $L$  and  $C$  resonate at the operating frequency; thus

$$U_{OUT} = \frac{1}{j\omega C} I_{IN} = -j\omega L I_{IN}. \quad (10)$$

TABLE II  
SUMMARY OF CONSTANT-VOLTAGE OUTPUT FROM A CURRENT SOURCE

Number	Passive resonant network	Resonant frequency
C-V-1		$\omega = \sqrt{\frac{1}{LC}}$
C-V-2		$\omega = \sqrt{\frac{1}{LC}}$

TABLE III  
SUMMARY OF CONSTANT-CURRENT OUTPUT FROM A VOLTAGE SOURCE

Number	Passive resonant network	Resonant frequency
V-C-1		$\omega = \sqrt{\frac{1}{LC}}$
V-C-2		$\omega = \sqrt{\frac{1}{LC}}$

The output voltage is load independent, which means it is determined only by the input current and can be adjusted by the resonant components. The type-B topology has a similar analysis process and results, i.e.,

$$U_{OUT} = j\omega LI_{IN} = -\frac{1}{j\omega C}I_{IN}. \quad (11)$$

The configurations for achieving constant-voltage output from a current source are listed in Table II.

**B. Constant-Current Output Principle**

In some charging applications, the voltage-to-current conversion and a load-independent current output are desirable. For instance, a constant-current output is preferred for driving a light-emitting diode for stable luminance [51]. The constant-current output is discussed below with different input sources.

1) *Input Voltage Source*: When the input is a voltage source and there is a constant-current output, it is the reverse conversion of the topologies listed in Fig. 3. Therefore, the resonant topology used to realize the conversion from a voltage source to a constant-current output should also have two types, as listed in Table III. The output currents are

$$\begin{aligned} \text{V-C-1: } I_{OUT} &= \frac{1}{j\omega L}U_{IN} = -j\omega CU_{IN} \\ \text{V-C-2: } I_{OUT} &= j\omega CU_{IN} = -\frac{1}{j\omega L}U_{IN}. \end{aligned} \quad (12)$$

2) *Input Current Source*: If the input is a current source, the resonant method for achieving a constant-current output is a  $\pi$ -circuit configuration, as shown in Fig. 4. Since it is similar to a constant-voltage output, to achieve a constant-current output from a current source, several typical compensation topologies can be derived by changing the connections of circuit points A, B, and C in Fig. 4(a) with circuit points a, b, and c in Fig. 4(b) or (c). The derivation is omitted for simplicity. The configurations are listed in Table IV.

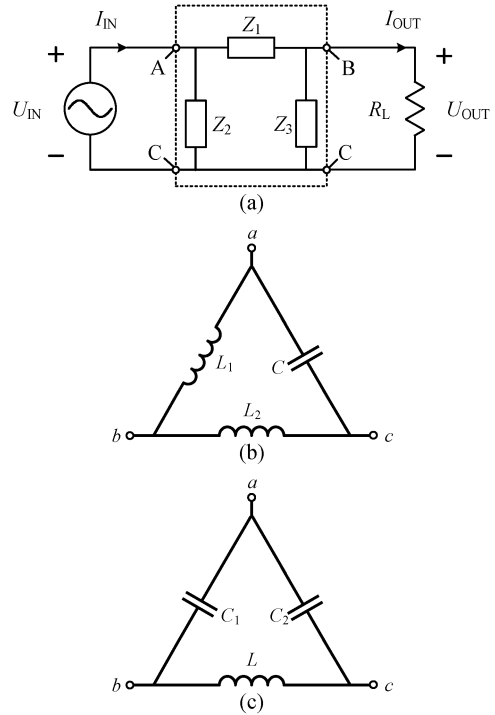


Fig. 4. Resonant network configuration with a (a)  $\pi$  circuit model, (b) type A, and (c) type B to have a constant-current output from a current source.

TABLE IV  
SUMMARY OF CONSTANT-CURRENT OUTPUT FROM A CURRENT SOURCE

Number	Passive resonant network	Resonant frequency
C-C-1		$\omega = \sqrt{\frac{1}{L_1C} + \frac{1}{L_2C}}$
C-C-2		$\omega = \frac{1}{\sqrt{LC_1 + LC_2}}$
C-C-3		$\omega = \frac{1}{\sqrt{LC_1 + LC_2}}$
C-C-4		$\omega = \frac{1}{\sqrt{LC_1 + LC_2}}$
C-C-5		$\omega = \sqrt{\frac{1}{L_1C} + \frac{1}{L_2C}}$
C-C-6		$\omega = \sqrt{\frac{1}{L_1C} + \frac{1}{L_2C}}$
C-C-7		$\omega = \frac{1}{\sqrt{LC}}$
C-C-8		---

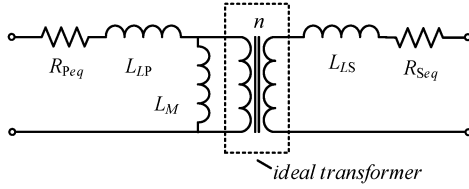


Fig. 5. Loosely coupled transformer circuit model.

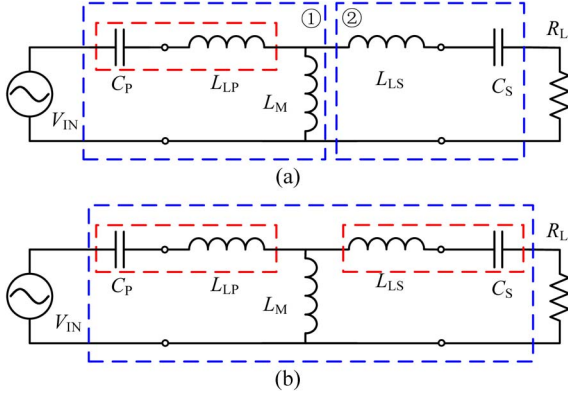


Fig. 6. Primary series and secondary series compensation circuit models to realize (a) constant-current and (b) constant-voltage output.

#### IV. APPLICATIONS AND EXAMPLES

Here, several typical compensation topologies that can achieve either a constant-voltage output or a constant-current output, or both, are analyzed by using the passive resonant networks studied in Section III. A WPT system has the same fundamental principle of magnetic induction as that of other widely used electromechanical devices with good coupling, such as transformers and induction motors; therefore, the circuit model of a loosely coupled transformer is identical to that of a traditional transformer, as shown in Fig. 5. In the analysis, the turn ratio  $n$  is selected as 1 for simplicity.  $L_{LP}$  and  $L_{LS}$  are the leakage inductances of the primary and secondary.  $L_M$  is the magnetizing inductance.  $R_{Peq}$  and  $R_{Seq}$  are the resistances of the primary and secondary of the transformer, respectively, including the winding resistance and the equivalent resistance of the power loss in the magnetic material. Since the values of  $R_{Peq}$  and  $R_{Seq}$  are relatively small compared with the compensation components' impedances and have limited influence on the resonant characteristic, they are neglected in this section.

##### A. Series-Series Compensation

1) *Constant-Current Output*: Primary series and secondary series (S/S) compensation, which is shown in Fig. 6, is one of the four basic compensation topologies [28], [40].  $C_P$  and  $C_S$  are external compensation capacitors in the primary and secondary. Let

$$\begin{aligned} Z_{LP}(\omega) &= j\omega L_{LP} + \frac{1}{j\omega C_P} \\ Z_{LS}(\omega) &= j\omega L_{LS} + \frac{1}{j\omega C_S}. \end{aligned} \quad (13)$$

The S/S compensation is designed to have a constant-current output [28], and the operating frequency is unique. This can be explained by the resonant networks in Section III. In Fig. 6(a), if  $Z_{LP}(\omega) < 0$  and the resonant tank in the red block is equivalent with a capacitor, which can resonate with  $L_M$ , then the block ① can be regarded as the resonant network V-C-2 in Table III, and a constant-current output is achieved in the branch circuit parallel with  $L_M$ . Therefore, the output current is constant regardless of the value of  $L_{LS}$ ,  $C_S$ , and  $R_L$ , since block ② can be regarded as the resonant circuit C-C-8 in Table IV, which has a constant-current output from the current source generated by block ①. The unique resonant frequency, to have a constant-current output, is

$$\omega = \omega_P = \frac{1}{\sqrt{(L_{LP} + L_M)C_P}} = \frac{1}{\sqrt{L_P C_P}} \quad (14)$$

where  $L_P$  is the self-inductance of the primary coil.

2) *Constant-Voltage Output*: The S/S topology can be also compensated to have a constant-voltage output, and the operating frequency for realizing a constant-voltage output is not unique. If we choose the compensation capacitors  $C_P$  and  $C_S$  randomly, two situations may exist.

- An operating frequency  $\omega_H$  can be found to have  $Z_{LP}(\omega) = Z_{LS}(\omega) = 0$ . Operating at  $\omega_H$ , the S/S topology can be regarded as the resonant circuit V-V-8 in Table I. If  $\omega_H$  exists, a frequency area should also exist, in which  $Z_{LP}(\omega) < 0$  and  $Z_{LS}(\omega) < 0$ . The series-connected resonant components in both primary and secondary are both equivalent with capacitors. A frequency  $\omega_L$  can be found to create the resonant circuit V-V-2 in Table I. Therefore,  $\omega_H$  and  $\omega_L$  are the two frequencies that realize a constant-voltage output.
- An operating frequency cannot be found to have  $Z_{LP}(\omega) = Z_{LS}(\omega) = 0$ . In this situation, the operating frequency can be adjusted within a certain range such that  $Z_{LP}(\omega) > 0$  and  $Z_{LS}(\omega) < 0$  or within a range such that  $Z_{LP}(\omega) < 0$  and  $Z_{LS}(\omega) > 0$ . Only one of these two scenarios can be achieved with one group of circuit parameters. Therefore, one operating frequency exists such that at  $\omega_H$ , the resonant circuit operates as V-V-5 (when  $Z_{LP}(\omega) > 0$  and  $Z_{LS}(\omega) < 0$ ) or V-V-6 (when  $Z_{LP}(\omega) < 0$  and  $Z_{LS}(\omega) > 0$ ) in Table I. In the meantime, with the same group of circuit parameters, another operating frequency can always be found to have  $Z_{LP}(\omega) < 0$  and  $Z_{LS}(\omega) < 0$ . Therefore, the other operating frequency exists such that at  $\omega_L$ , the resonant circuit operates as V-V-2 in Table I.

These two frequencies can be also derived by using mathematical equations. To make sure the derivation is applicable for general loosely coupled transformers instead of those with  $n = 1$ , the turn ratio is introduced in the following analysis. In the following figures, the transformer with  $n = 1$  is maintained to have a clear explanation of the blocks of resonant circuits in Section III.

The output voltage on  $R_L$  is calculated as

$$U_{OUT} = U_{IN} G_v \quad (15)$$

where  $G_v$  is the voltage transfer ratio, which can then be represented as

$$G_v = \frac{U_{\text{OUT}}}{U_{\text{IN}}} = \frac{j\omega n L_M R_L}{Z_P Z_S + n^2 \omega^2 L_M^2} \quad (16)$$

where  $Z_S$  is the impedance of the secondary resonant tank including load resistance  $R_L$ .  $Z_P$  is the impedance of the primary resonant tank, where  $L_P$  and  $L_S$  are the self-inductances, i.e.,

$$Z_S = j\omega L_S + \frac{1}{j\omega C_S} + R_L$$

$$Z_P = j\omega L_P + \frac{1}{j\omega C_P}. \quad (17)$$

The voltage transfer characteristics can be obtained by further manipulation of (16), i.e.,

$$|G_v| = \frac{1}{\frac{Z_P}{\omega n L_M} + \frac{\delta}{\omega^3 n L_M C_P C_S R_L}} \quad (18)$$

$$\delta = \omega^4 L_P C_P L_S C_S (k^2 - 1) + \omega^2 (L_P C_P + L_S C_S) - 1 \quad (19)$$

where  $k = n L_M / \sqrt{L_P L_S}$  is the coupling coefficient of the loosely coupled transformer. Equation (19) shows that if  $\delta = 0$ , then  $|G_v|$  is load independent, and the output voltage remains constant when  $R_L$  changes. Solving for roots of  $\delta = 0$ , the frequencies at which  $|G_v|$  is independent of  $R_L$  can be obtained as

$$\omega_L = \sqrt{\frac{\omega_P^2 + \omega_S^2 - \Delta}{2(1 - k^2)}} \quad (20)$$

$$\omega_H = \sqrt{\frac{\omega_P^2 + \omega_S^2 + \Delta}{2(1 - k^2)}} \quad (21)$$

$$\Delta = \sqrt{(\omega_P^2 + \omega_S^2)^2 - 4(1 - k^2)\omega_P^2\omega_S^2} \quad (22)$$

where  $\omega_s = 1/\sqrt{L_S C_S}$  is the resonant frequencies of  $L_S$  and  $C_S$ .  $L_S$  is the self-inductance of the secondary coil. Thus, the existence of  $\omega_L$  and  $\omega_H$  is mathematically verified.

Research [44] is conducted to compare self-inductance compensation and leakage inductance compensation. The only difference between the two compensations is the capacitors' values. Therefore, according to the given analysis, both types of compensation can achieve constant-voltage/constant-current output but operating at different frequencies.

### B. Series-Parallel Compensation

Primary series and secondary parallel (S/P) compensation is usually designed to have a constant-voltage output. In Fig. 7(a), if  $Z_{LP}(\omega) < 0$ , the S/P compensation topology can be regarded as the combination of the resonant network V-V-6 in block ① and V-V-8 in block ②. A constant-voltage output can be achieved only when operating at

$$\omega = \sqrt{\frac{1}{C_P \left( L_{LP} + \frac{L_M L_{LS}}{L_M + L_{LS}} \right)}} \quad (23)$$

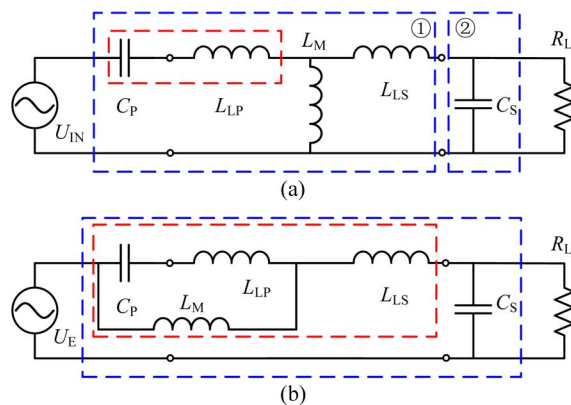


Fig. 7. S/P compensation circuit models to have (a) constant-voltage and (b) constant-current output (Thévenin's equivalent circuit).

S/P compensation can also realize a constant-current output. By further manipulation using Thévenin's equivalent circuit, the S/P compensation topology can be reorganized as Fig. 7(b), which illustrates the constant-current output.  $U_E$  is the equivalent input voltage after Thévenin's conversion, i.e.,

$$U_E = U_{\text{IN}} \frac{j\omega L_M}{Z_P}. \quad (24)$$

If the operating frequency is selected to let the impedance in the red dotted block perform as an equivalent inductor, which can resonate with  $C_S$ , it can be regarded as the resonant circuit V-C-1 in Table III, and the output current is constant. The transconductance ratio can be derived as

$$|G_i| = \frac{I_{\text{OUT}}}{U_{\text{IN}}} = \frac{1}{\omega n L_M + \frac{j\omega L_S Z_P}{\omega n L_M} + \gamma R_L} \quad (25)$$

where

$$\gamma = j\omega^2 n L_M C_S + \frac{Z_P(1 - \omega^2 L_S C_S)}{\omega n L_M}. \quad (26)$$

Similarly, operating at frequencies at which  $\gamma = 0$  guarantees that  $I_O$  is independent of  $R_L$ . It has been found that  $\omega_L$  and  $\omega_H$  in (20) and (21) are also the two roots of  $\gamma = 0$  [46]. Therefore,  $\omega_L$  and  $\omega_H$  are the frequencies at which S/P compensation achieves a load-independent current output.

### C. Primary LCC Compensations

The primary LCC series-parallel compensations are designed for a WPT system with multiple loadings, such as roadway-powered vehicle IPT systems, which are composed of a primary track made up of an elongated loop as the primary of the loosely coupled transformer. The primary track is required to provide power to a number of independent loads (EVs) wirelessly, each of which couples to the track using a pickup inductor placed in proximity to the track wires. Therefore, the track current is always preferred to be constant to guarantee constant power delivery to each pickup system [5], [29].

A series of primary LCC series-parallel compensations, as shown in Fig. 8, is widely used for the track WPT system design [29], [48].  $I_{\text{track}}$  is the current through the track, and the



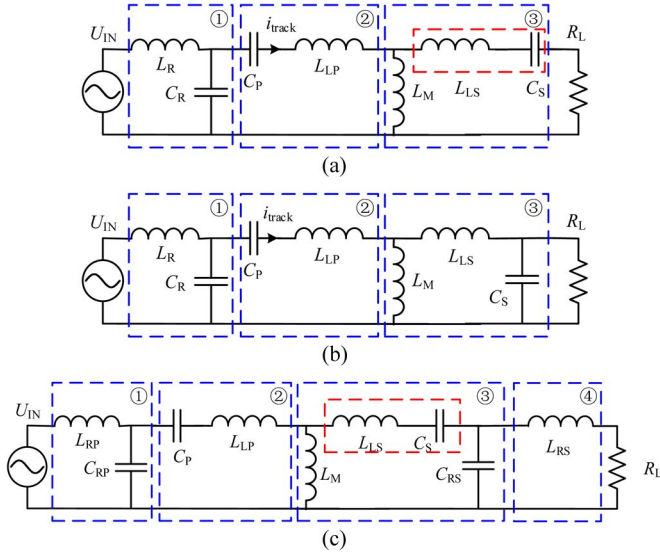


Fig. 8. Primary LCC series-parallel compensation circuit models with (a) secondary series compensation, (b) secondary parallel compensation, and (c) secondary LCC compensation.

design purpose is to maintain  $I_{\text{track}}$  constant during operation. In the meantime, each load powered by the track should have a constant-voltage or constant-current output.

All primary LCC series-parallel compensations will have a constant-current output in the primary coil if  $L_R$  and  $C_R$  in block ① are selected to resonate at the operating frequency of the converter. The primary LCC series-parallel compensation topology block ① shown in Fig. 8 can be regarded as the resonant circuit V-C-1 in Table III. Since the constant-current output of the primary coil (track) can be regarded as a current source, block ② is the resonant circuit C-C-8. In the secondary of the transformer, if a constant voltage is achieved on the load, a compensation capacitor should be connected in series with the secondary coil, as shown in Fig. 8(a). In Fig. 8(a), block ③ is C-V-1 while  $C_S$  resonates with  $L_M + L_{LS}$ . Therefore, the constant-voltage output requires

$$\omega = \frac{1}{\sqrt{(L_{LS} + L_M)C_S}} = \frac{1}{\sqrt{L_S C_S}} = \frac{1}{\sqrt{L_R C_R}}. \quad (27)$$

If the compensation capacitor is connected in parallel with the secondary coil as shown in Fig. 8(b), where resonant network C-C-1 is formed in block ③, a constant-current output can be achieved when satisfying (27). A double-sided LCC compensation topology shown in Fig. 8(c) is proposed in [52], which has a symmetrical compensation in the primary and secondary. By adding a capacitor in block ③ C-C-1 and block ④ C-C-8, a constant-current output is achieved.

In battery charger applications, an additional converter is usually placed on the secondary side to manage a battery load profile (a first step at constant-current output and a second step at constant-voltage output) [53]. By using appropriate compensations and operating frequency selection control, voltage or current conversion can be achieved by a single stage of a WPT converter.

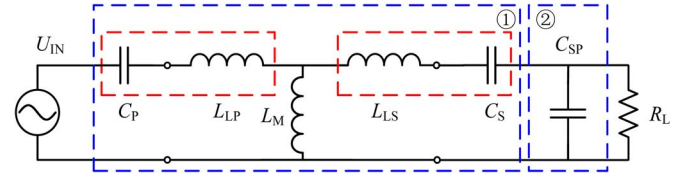


Fig. 9. S/SP compensation circuit model.

## V. ZPA AND SOFT SWITCHING

The phase angle  $\theta_{\text{in}}$  between the input voltage and current is an important parameter that decides on the VA rating of the power supply and of the switching components. It also relates to the realization of soft switching of an H-bridge converter. The minimum VA rating requires that  $\theta_{\text{in}}$  is equal to zero, whereas soft switching of MOSFETs requires that  $\theta_{\text{in}}$  is larger than zero. Therefore,  $\theta_{\text{in}}$  is usually selected such that it is slightly greater than zero, so as to realize soft switching and a reasonable VA rating.

The input phase angle is calculated as

$$\theta_{\text{in}} = \frac{180}{\pi} \tan^{-1} \frac{\text{Im}(Z_{\text{in}})}{\text{Re}(Z_{\text{in}})}. \quad (28)$$

We study the situation of  $\theta_{\text{in}} = 0$ . It can be achieved when  $\text{Im}(Z_{\text{in}}) = 0$ .

According to the analysis of passive resonant networks in Section III, due to the change in value of the loading resistance, which is connected in parallel with one of the resonant components, it is impossible to keep  $\theta_{\text{in}} = 0$  with only one stage of the passive resonant network. Two special topologies, namely, V-V-7 and C-C-7, are special exceptions. Take the S/S compensation topology as an example. In Fig. 6(b), if the S/S compensation is designed to have a constant-voltage output, since it has only one stage of the resonant block, the value of  $\theta_{\text{in}}$  is dependent on the value of loading resistances.  $\theta_{\text{in}}$  can be positive or negative with variable  $R_L$  [54]. Therefore, the S/S compensation topology cannot realize a ZPA when it has the constant-voltage output.

If a load-independent voltage/current output and  $\theta_{\text{in}} = 0$  at the full loading range are realized at the same time, two or more stages of the resonant circuit studied in Section III are needed. As shown in Fig. 6(a), when an S/S compensation has a constant-current output, it is the combination of two resonant networks V-C-2 and C-C-8. Stage C-C-8 does not contribute to the creation of a constant-current output, but it is capable of adjusting the value of  $\theta_{\text{in}}$ . Therefore, the S/S compensation can have an input ZPA and a constant-current output at the same time [46].

A primary series and secondary series-parallel compensated topology (S/SP) is proposed as an improvement for the S/S compensation topology to have a ZPA and a constant-voltage output simultaneously [55]. In the S/SP circuit shown in Fig. 9,  $C_P$  and  $C_S$  are selected the same to form the resonant network in Fig. 6(b), a secondary parallel-connected capacitor  $C_{SP}$  is added to realize another stage of V-V-8. This stage has no contribution to the constant-voltage output, but  $\theta_{\text{in}}$  of this S/SP

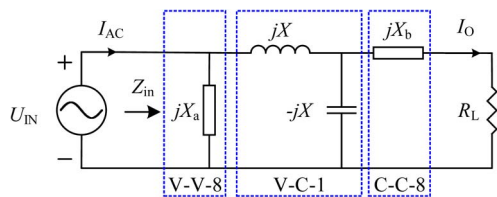


Fig. 10. Two or more stages (including V-C-1) to have a constant-current output and an input ZPA.

compensation is controlled and adjusted by  $C_{SP}$  to realize soft switching, i.e.,

$$C_{SP} = \frac{1}{\omega^2 n^2 L_M}. \quad (29)$$

Similarly, S/P compensation also has this problem. For the resonant circuit V-C-1 in Fig. 7(b), which is the single stage adapted to have a constant-current output, another stage of resonant network is needed to achieve a ZPA for all loads and load-independent current output simultaneously. Fig. 10 shows the resonant network with V-C-1 and the other stage. The other stage can be added either before or after the V-C-1 stage. We add them both for the analysis to include all possible circuit topologies. In practice,  $jX_a = \infty$  or  $jX_b = 0$  can be selected to represent one stage.

Since the inductor and capacitor in stage V-C-1 resonate with each other, let

$$X = \omega L = \frac{1}{\omega C} \quad (30)$$

$$Z_{in} = \frac{R_L X^2 X_a^2 + jX^2 X_a [X^2 + X_a(X - X_b)]}{[X^2 + X_a(X - X_b)]^2 + R_L^2 X_a^2}. \quad (31)$$

If  $X_a \rightarrow \infty$ , then C-C-8 has been added behind the V-C-1 stage, i.e.,

$$Z_{in}|_{X_a \rightarrow \infty} = \frac{R_L X^2 + jX^2(X - X_b)}{R_L^2}. \quad (32)$$

To realize  $\text{Im}(Z_{in}) = 0$  and  $\theta_{in} = 0$ ,  $X_b$  should be equal to  $X$ . If  $X_b = 0$ , then V-V-8 has been added before the V-C-1 stage, and

$$Z_{in}|_{X_b=0} = \frac{R_L X^2 X_a^2 + jX^2 X_a [X^2 + X_a X]}{[X^2 + X_a X]^2 + R_L^2 X_a^2}. \quad (33)$$

For  $\theta_{in}$  to be equal to 0,  $X_a$  should be equal to  $-X$ . If the stages of both V-V-8 and C-C-8 are added, then according to (31), the impedances should satisfy

$$X^2 + X_a(X - X_b) = 0 \quad (34)$$

to make  $\theta_{in} = 0$  for all loading conditions.

For all the primary LCC series-parallel compensations, since they also utilize the V-C-1 or V-C-2 resonant networks to realize a constant-current output in the primary coil, the series-connected capacitor  $C_P$  (see Fig. 8) can be regarded as one

more stage C-C-8. This stage has no contribution of constant-current output but is added to adjust  $\theta_{in}$ . According to (31), a ZPA can be achieved when

$$C_P = \frac{C_R}{\frac{L_P}{L_R} - 1}. \quad (35)$$

## VI. SYSTEM EFFICIENCY

To calculate system efficiency, the resistances  $R_{Peq}$  and  $R_{Seq}$  in Fig. 5 should be considered. Then,  $Z_P$  and  $Z_S$  are redefined as

$$\begin{aligned} Z_S &= j\omega L_S + \frac{1}{j\omega C_S} + R_{Seq} + R_L \\ Z_P &= j\omega L_P + \frac{1}{j\omega C_P} + R_{Peq}. \end{aligned} \quad (36)$$

The expression of power transfer efficiency can be obtained by solely considering the active power [46], [53], and thus, the efficiency  $\eta_P$  of the primary loop and the efficiency  $\eta_S$  of the secondary loop can be calculated separately as

$$\eta_P = \frac{\text{Re}(Z_{ref})}{R_{Peq} + \text{Re}(Z_{ref})} \quad (37)$$

$$\eta_S = \frac{\text{Re}(Z_S) - R_{Seq}}{\text{Re}(Z_S)} \quad (38)$$

where  $Z_{ref}$  is the reflected impedances from the secondary to the primary. Thus

$$Z_{ref} = \frac{\omega^2 n^2 L_M^2}{Z_S}. \quad (39)$$

Efficiency  $\eta$  is therefore given by

$$\eta = \eta_P \cdot \eta_S. \quad (40)$$

In (37)–(40), the circuit efficiency is related to  $R_{Peq}$ ,  $R_{Seq}$ ,  $nL_M$ , and  $Z_S$ . If the operating frequency is fixed or varies in a narrow region,  $R_{Peq}$ ,  $R_{Seq}$  is related with the selected electric wire and the magnetic material.  $nL_M$  represents the mutual inductance and is determined by the coupling coefficient of the transformer. These parameters can be regarded as fixed when the loosely coupled transformer is built; they are not discussed in this paper. Therefore,  $Z_S$  is the only parameter that determines the circuit efficiency. If the compensation capacitors have no equivalent series resistance (ESR), in (37)–(40), the efficiency does not depend on the primary compensation network. Compensation in the primary only influences the reactive power of the circuit, the VA rating of the input power source, and the realization of soft switching. From (36),  $Z_S$  is decided by 1) the impedance of the secondary resonant network and 2) the value of loading resistance. For a given transformer, the maximum circuit efficiency can be achieved by adjusting these two parameters deciding  $Z_S$ .

With regard to the impedance of the secondary resonant network, the compensation capacitor should be well designed



to achieve the maximum efficiency. According to the study in [46] and [53], the maximum efficiency appears when

$$\begin{aligned} \text{secondary series compensation } C_S &= \frac{1}{\omega^2 L_S} \\ \text{secondary parallel compensation } C_S &= \frac{1}{\omega^2 L_S \Gamma^2} \end{aligned} \quad (41)$$

where

$$\Gamma = \left(1 + \frac{Q_P k^2}{Q_S}\right)^{\frac{1}{4}} \quad (42)$$

and  $Q_P$  and  $Q_S$  are defined as the winding quality factors, which can be expressed as

$$Q_P = \frac{\omega L_P}{R_{P\text{eq}}} \quad \text{and} \quad Q_S = \frac{\omega L_S}{R_{S\text{eq}}} \quad (43)$$

Therefore, to achieve the maximum efficiency, the capacitor in the secondary resonant network should be designed as in (41). With regard to the loading resistance, if  $R_L$  is expressed by the circuit quality factor  $Q_L$ , according to the study in [46] and [54], to achieve the maximum efficiency,  $Q_L$  should satisfy

$$Q_L = \frac{Q_S}{\sqrt{1 + k^2 Q_P Q_S}} \quad (44)$$

for both secondary series and parallel compensations. The circuit quality factor  $Q_L$  in (44) has a different expression for secondary series and parallel compensations. Thus

$$\begin{aligned} \text{secondary series compensation } Q_L &= \frac{1}{R_L} \sqrt{\frac{L_S}{C_S}} \\ \text{secondary parallel compensation } Q_L &= R_L \sqrt{\frac{C_S}{L_S}} \end{aligned} \quad (45)$$

Therefore, considering the need to achieve maximum efficiency, secondary series and parallel compensations have varying applications. For instance, in EV battery wireless charging, suppose the battery on board has a voltage of 400 V and an internal resistance of 0.7  $\Omega$ . If the recharging power is 3.3 kW for private cars, by simple derivation, the output voltage and current of the wireless converter should be 405.7 V and 8.13 A. Therefore, the equivalent loading resistance  $R_L$  is 49.9  $\Omega$ . Typically, the winding quality factors  $Q_P$  and  $Q_S$  can reach 200 by using a proper litz wire, and we assume the coupling coefficient to be 0.2. According to (44),  $Q_L$  can be calculated to have a value of 5. From (45), if secondary series compensation is selected,  $L_S$  is equal to 468  $\mu\text{H}$  when the converter operates at 85 kHz. If secondary parallel compensation is selected,  $L_S$  should be designed as 18  $\mu\text{H}$ . For the coil to be installed on the chassis of a vehicle and with  $k = 0.2$ , 18  $\mu\text{H}$  is not a reasonable value. Therefore, secondary series compensation is more suitable for this EV wireless charging example to achieve maximum efficiency.

Generally, when considering the ESRs of compensation conductors and capacitors, the more compensation components there are, the lower the circuit efficiency. S/S and S/P compensation circuits have the highest efficiencies due to only two compensation components being applied. The system with

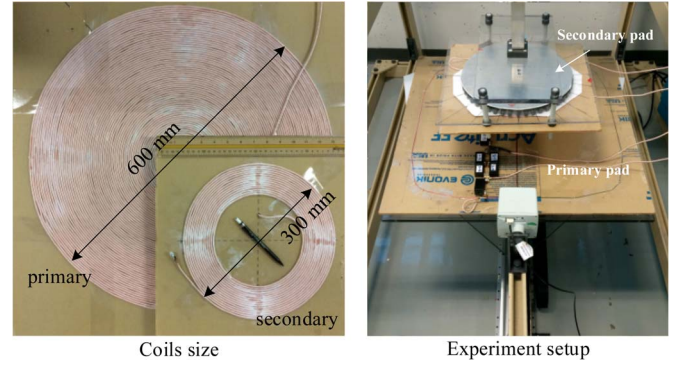


Fig. 11. Loosely coupled transformer prototype.

TABLE V  
SPECIFICATIONS OF THE LOOSELY COUPLED TRANSFORMER PROTOTYPE

Transformer & circuit parameters		Specifications
Coil topology		Unipolar
coil	primary	Circular, 600 mm dia., 32 turns, litz wire with 800 strands AWG38, two wires connected in parallel as one turn, $L_P = 420 \mu\text{H}$
	secondary	Circular, 300 mm dia., 16 turns, litz wire with 800 strands AWG38, $L_S = 110 \mu\text{H}$
core	primary	48 bars of PC40 with 8mm thickness, same external diameter with the primary coil.
	secondary	48 bars of PC40 with 8mm thickness, same external diameter with the secondary coil.
Shieldings		2 mm aluminum circular sheet, same size with the coil
Air gap		150 mm
Coupling coefficient		0.182
Output power		3.3 kW
Battery voltage		400 V
Input voltage		350 V
Operating frequency		85 kHz

S/S and S/P compensations has almost the same maximum efficiency [46], and  $\eta_{\text{max}}$  can be represented as

$$\begin{aligned} \eta_{\text{max}} &= \frac{c}{(1 + \sqrt{1 + c})^2} \\ c &= k^2 Q_P Q_S \end{aligned} \quad (46)$$

This  $\eta_{\text{max}}$  value can be achieved when both (41) and (44) are satisfied. It relates only to the values of  $k$  and the winding quality factors.

A loosely coupled transformer shown in Fig. 11 was built to verify the circuit efficiency of a 3.3-kW stationary EV wireless charging prototype. The specifications of the transformer is listed in Table V. Based on the built transformer, to calculate the system efficiency, we select the quality factor of the transformer  $Q_P = Q_S = 200$ , which is a typical value for a loosely coupled transformer operating around 85 kHz. The double-sided LCC compensation topology aforementioned in Fig. 8(c) is used for the experiment. For the compensation inductor in the circuits, since it uses the same wire with the loosely coupled transformer, the quality factor of the resonant

TABLE VI  
MAXIMUM EFFICIENCIES OF DIFFERENT COMPENSATION TOPOLOGIES

Compensation topology	Maximum efficiency	Constant output type
Series-series	94.6%	current
Series-parallel	94.6%	voltage
Series-series with leakage inductance compensation	93.3%	voltage
LCC-series	94.2%	voltage
LCC-parallel	94.3%	current
LCC-LCC	93.5%	current

inductor is also selected as 200, and the capacitor have a dissipation factor of 0.05% based on the datasheet. The circuit efficiency is measured and calculated. The calculated system efficiency (dc–dc) is 93.6%, whereas the measured efficiency is 92.6%. The consistency of measurement with calculation verifies that  $Q_P$ ,  $Q_S$ , and the ESR values of the compensation components are accurate.

Based on the same loosely coupled transformer and the same compensation component ESR values, the efficiency of various compensation topologies is calculated and listed in Table VI. It is proved that S/S and S/P compensations have better efficiencies than other topologies, as well as the accuracy of (46).

The efficiency of the S/S topology with leakage-inductance compensation is calculated under the condition of constant-voltage output since it is the original purpose [44]. The operating frequency having a constant-voltage output is  $\omega_L$  or  $\omega_H$  in (19) and (20), instead of the secondary resonant frequency in (41) at which the maximum efficiency can be achieved. Therefore, the S/S topology with leakage-inductance compensation, to have a constant-voltage output, is lower in efficiency than self-inductance compensation, to have a constant-current output.

## VII. CONCLUSION

The constant-current/constant-voltage output function of a passive resonant network has been introduced based on individual resonant blocks. These basic resonant blocks are used to explain some characteristics of popular compensation topologies nowadays, such as constant-voltage or constant-current output and the realization of an input ZPA, as well as soft switching. By correctly combining these resonant blocks, any type of compensation topology can be created, guaranteeing a WPT circuit that achieves a constant output and a minimum input VA rating simultaneously. In addition, system efficiency was analyzed with different resonant circuits. The compensation conditions, to achieve maximum efficiency, were reviewed. The WPT system application area should be considered for a reasonable circuit design to achieve this maximum efficiency. Furthermore, primary-series and secondary-series topologies with leakage-inductance compensation and self-inductance compensation were studied and compared.

## REFERENCES

- [1] 2014. [Online]. Available: <http://en.wikipedia.org/wiki/Wardenclyffe>
- [2] N. Tesla, Apparatus for Transmitting Electrical Energy, U.S. Patent 1 119 732, Dec. 1, 1914.
- [3] N. Tesla, *My Inventions: The Autobiography of Nikola Tesla*. Rockville, MD, USA: Wildside Press, 2005.
- [4] R. Lomas, *The Man Who Invented the Twentieth Century: Nikola Tesla, Forgotten Genius of Electricity*. London, U.K.: Headline Book Publ., 2000.
- [5] G. A. Covic and J. T. Boys, "Inductive Power Transfer," in *Proc. IEEE*, vol. 101, no. 6, pp. 1276–1289, Jun. 2013.
- [6] S. Y. R. Hui and W. C. Ho, "A new generation of universal contactless battery charging platform for portable consumer electronic equipment," *IEEE Trans. Power Electron.*, vol. 20, no. 3, pp. 620–627, May 2005.
- [7] S. Y. Hui, "Planar wireless charging technology for portable electronic products and Qi," *Proc. IEEE*, vol. 101, no. 6, pp. 1290–1301, Jun. 2013.
- [8] L. Xun and S. Y. R. Hui, "Equivalent circuit modeling of a multilayer planar winding array structure for use in a universal contactless battery charging platform," *IEEE Trans. Power Electronics*, vol. 22, no. 1, pp. 21–29, Jan. 2007.
- [9] L. Xun and S. Y. R. Hui, "Optimal design of a hybrid winding structure for planar contactless battery charging platform," *IEEE Trans. Power Electron.*, vol. 23, no. 1, pp. 455–463, Jan. 2008.
- [10] L. Xun and S. Y. R. Hui, "Simulation study and experimental verification of a universal contactless battery charging platform with localized charging features," *IEEE Trans. Power Electron.*, vol. 22, no. 6, pp. 2202–2210, Nov. 2007.
- [11] C.-G. Kim, D.-H. Seo, J.-S. You, J.-H. Park, and B. H. Cho, "Design of a contactless battery charger for cellular phone," *IEEE Trans. Ind. Electron.*, vol. 48, no. 6, pp. 1238–1247, Dec. 2001.
- [12] E. Waffenschmidt and T. Staring, "Limitation of inductive power transfer for consumer applications," in *Proc. 13th Eur. Conf. Power Electron. Appl.*, 2009, pp. 1–10.
- [13] J. Yungtaek and M. M. Jovanovic, "A contactless electrical energy transmission system for portable-telephone battery chargers," *IEEE Trans. Ind. Electron.*, vol. 50, no. 3, pp. 520–527, Jun. 2003.
- [14] T. D. Dissanayake *et al.*, "Experimental study of a TET system for implantable biomedical devices," *IEEE Trans. Biomed. Circuits Syst.*, vol. 3, no. 6, pp. 370–378, Dec., 2009.
- [15] L. Ho Yan, D. M. Budgett, and A. P. Hu, "Minimizing power loss in air-cored coils for TET heart pump systems," *IEEE J. Emerging Sel. Topics Circuits Syst.*, vol. 1, no. 3, pp. 412–419, Sep. 2011.
- [16] T.-H. Nishimura *et al.*, "A large air gap flat transformer for a transcutaneous energy transmission system," in *Proc. 25th IEEE PESC/IEEE Power Electron. Spec. Conf.*, 1994, pp. 1323–1329.
- [17] T. Takura, H. Ishiai, F. Sato, H. Matsuki, and T. Sato, "Basic evaluation of signal transmission coil in transcutaneous magnetic telemetry system for artificial hearts," *IEEE Trans. Magn.*, vol. 41, no. 10, pp. 4173–4175, Oct. 2005.
- [18] H. Miura *et al.*, "Improvement of the transcutaneous energy transmission system utilizing ferrite cored coils for artificial hearts," *IEEE Trans. Magn.*, vol. 42, no. 10, pp. 3578–3580, Oct. 2006.
- [19] A. Ghahary and B. H. Cho, "Design of transcutaneous energy transmission system using a series resonant converter," *IEEE Trans. Power Electron.*, vol. 7, no. 2, pp. 261–269, Apr. 1992.
- [20] J. Gyu Bum and B. H. Cho, "An energy transmission system for an artificial heart using leakage inductance compensation of transcutaneous transformer," *IEEE Trans. Power Electron.*, vol. 13, no. 6, pp. 1013–1022, Nov. 1998.
- [21] M. L. G. Kissin, H. Hao, and G. A. Covic, "A practical multiphase IPT system for AGV and roadway applications," in *Proc. IEEE ECCE*, 2010, pp. 1844–1850.
- [22] A. Zaheer, M. Budhia, D. Kacprzak, and G. A. Covic, "Magnetic design of a 300 W under-floor contactless power transfer system," in *Proc. 37th Annu. Conf. IEEE Ind. Electron. Soc.*, 2011, pp. 1408–1413.
- [23] P. Basset, A. Kaiser, B. Legrand, D. Collard, and L. Buchaillet, "Complete system for wireless powering and remote control of electrostatic actuators by inductive coupling," *IEEE/ASME Trans. Mechatron.*, vol. 12, no. 1, pp. 23–31, Feb. 2007.
- [24] B. de Jeroen, E. A. Lomonova, and A. J. A. Vandenput, "Optimization of contactless planar actuator with manipulator," *IEEE Trans. Magn.*, vol. 44, no. 6, pp. 1118–1121, Jun. 2008.
- [25] W. Zhang, S.-C. Wong, C. K. Tse, and Q. Chen, "An optimized track length in roadway inductive power transfer systems," *IEEE J. Emerging Sel. Topics Power Electron.*, vol. 2, no. 3, pp. 598–608, Sep. 2014.

- [26] J. L. Villa, J. Sallán, A. Llombart, and J. F. Sanz, "Design of a high frequency inductively coupled power transfer system for electric vehicle battery charge," *Appl. Energy*, vol. 86, no. 3, pp. 355–363, Mar. 2009.
- [27] F. Musavi, M. Edington, and W. Eberle, "Wireless power transfer: A survey of EV battery charging technologies," in *Proc. IEEE ECCE*, 2012, pp. 1804–1810.
- [28] C.-S. Wang, O. H. Stielau, and G. A. Covic, "Design considerations for a contactless electric vehicle battery charger," *IEEE Trans. Ind. Electron.*, vol. 52, no. 5, pp. 1308–1314, Oct. 2005.
- [29] G. A. Covic and J. T. Boys, "Modern trends in inductive power transfer for transportation applications," *IEEE J. Emerging Sel. Top. Power Electron.*, vol. 1, no. 1, pp. 28–41, Mar. 2013.
- [30] J. Huh *et al.*, "Narrow-width inductive power transfer system for on-line electrical vehicles," *IEEE Trans. Power Electron.*, vol. 26, no. 12, pp. 3666–3679, Dec. 2011.
- [31] M. L. G. Kissin, J. T. Boys, and G. A. Covic, "Interphase mutual inductance in polyphase inductive power transfer systems," *IEEE Trans. Ind. Electron.*, vol. 56, no. 7, pp. 2393–2400, Jul. 2009.
- [32] M. L. G. Kissin, G. A. Covic, and J. T. Boys, "Steady-state flat-pickup loading effects in polyphase inductive power transfer systems," *IEEE Trans. Ind. Electron.*, vol. 58, no. 6, pp. 2274–2282, Jun. 2011.
- [33] N. H. Kutkut, D. M. Divan, D. W. Novotny, and R. H. Marion, "Design considerations and topology selection for a 120-kW IGBT converter for EV fast charging," *IEEE Trans. Power Electron.*, vol. 13, no. 1, pp. 169–178, Jan. 1998.
- [34] S. Lee *et al.*, "On-line electric vehicle using inductive power transfer system, in *Proc. IEEE ECCE*, 2010, pp. 1598–1601.
- [35] S. Lee, B. Choi, and C. T. Rim, "Dynamics characterization of the inductive power transfer system for online electric vehicles by Laplace phasor transform," *IEEE Trans. Power Electron.*, vol. 28, no. 12, pp. 5902–5909, Dec. 2013.
- [36] F. Sato *et al.*, "Contactless energy transmission to mobile loads by CLPS—Test driving of an EV with starter batteries," *IEEE Trans. Magn.*, vol. 33, no. 5, pp. 4203–4205, Sep. 1997.
- [37] J. Garnica, R. A. Chinga, and L. Jenschan, "Wireless power transmission: From far field to near field," *Proc. IEEE*, vol. 101, no. 6, pp. 1321–1331, Jun. 2013.
- [38] A. Ghahary and B. H. Cho, "Design of a transcutaneous energy transmission system using a series resonant converter," in *Proc. 21st Annu. IEEE Power Electron. Spec. Conf.*, 1990, pp. 1–8.
- [39] R. W. Erickson and D. Maksimovic, *Fundamentals of Power Electronics*. New York, NY, USA: Springer-Verlag, 2001.
- [40] C.-S. Wang, G. A. Covic, and O. H. Stielau, "Power transfer capability and bifurcation phenomena of loosely coupled inductive power transfer systems," *IEEE Trans. Ind. Electron.*, vol. 51, no. 1, pp. 148–157, Feb. 2004.
- [41] C.-S. Wang, G. A. Covic, and O. H. Stielau, "Investigating an LCL load resonant inverter for inductive power transfer applications," *IEEE Trans. Power Electron.*, vol. 19, no. 4, pp. 995–1002, Jul. 2004.
- [42] N. A. Keeling, G. A. Covic, and J. T. Boys, "A unity-power-factor IPT pickup for high-power applications," *IEEE Trans. Ind. Electron.*, vol. 57, no. 2, pp. 744–751, Feb. 2010.
- [43] G. A. J. Elliott, G. A. Covic, D. Kacprzak, and J. T. Boys, "A new concept: Asymmetrical pick-ups for inductively coupled power transfer monorail systems," *IEEE Trans. Magn.*, vol. 42, no. 10, pp. 3389–3391, Oct. 2006.
- [44] Q. Chen, S. C. Wong, and X. Ruan, "Analysis, design, and control of a transcutaneous power regulator for artificial hearts," *IEEE Trans. Biomed. Circuits Syst.*, vol. 3, no. 1, pp. 23–31, Feb. 2009.
- [45] M. Pinuela, D. C. Yates, S. Lucyszyn, and P. D. Mitcheson, "Maximizing dc-to-load efficiency for inductive power transfer," *IEEE Trans. Power Electron.*, vol. 28, no. 5, pp. 2437–2447, May 2013.
- [46] W. Zhang, S.-C. Wong, C. K. Tse, and Q. Chen, "Analysis and comparison of secondary series- and parallel-compensated inductive power transfer systems operating for optimal efficiency and load-independent voltage-transfer ratio," *IEEE Trans. Power Electron.*, vol. 29, no. 6, pp. 2979–2990, Jun. 2014.
- [47] R. L. Steigerwald, "A comparison of half-bridge resonant converter topologies," *IEEE Trans. Power Electron.*, vol. PEL-3, no. 2, pp. 174–182, Apr. 1988.
- [48] Z. Pantic, B. Sanzhong, and S. Lukic, "ZCS LCC-compensated resonant inverter for inductive-power-transfer application," *IEEE Trans. Ind. Electron.*, vol. 58, no. 8, pp. 3500–3510, Aug. 2011.
- [49] G. A. Covic, J. T. Boys, M. L. G. Kissin, and H. G. Lu, "A three-phase inductive power transfer system for roadway-powered vehicles," *IEEE Trans. Ind. Electron.*, vol. 54, no. 6, pp. 3370–3378, Dec. 2007.
- [50] J. Sallan, J. L. Villa, A. Llombart, and J. F. Sanz, "Optimal design of ICPT systems applied to electric vehicle battery charge," *IEEE Trans. Ind. Electron.*, vol. 56, no. 6, pp. 2140–2149, Jun. 2009.
- [51] X. Qu, W. Zhang, S.-C. Wong, and C. K. Tse, "Design of a current-source-output inductive power transfer led lighting system," *IEEE J. Emerging Sel. Topics Power Electron.*, vol. 3, no. 1, pp. 306–314, Mar. 2015.
- [52] S. Li, W. Li, J. Deng, T. D. Nguyen, and C. C. Mi, "A double-sided LCC compensation network and its tuning method for wireless power transfer," *IEEE Trans. Veh. Technol.*, vol. 64, no. 6, pp. 2261–2273, Jun. 2015.
- [53] M. Yilmaz and P. T. Krein, "Review of battery charger topologies, charging power levels, and infrastructure for plug-in electric and hybrid vehicles," *IEEE Trans. Power Electron.*, vol. 28, no. 5, pp. 2151–2169, May 2013.
- [54] W. Zhang, S.-C. Wong, and Q. Chen, "Design for efficiency optimization and voltage controllability of series-series compensated inductive power transfer systems," *IEEE Trans. Power Electron.*, vol. 29, no. 1, pp. 191–200, Jan. 2014.
- [55] J. Hou *et al.*, "Precise characteristics analysis of series/series-parallel compensated contactless resonant converter," *IEEE J. Emerging Sel. Topics Power Electron.*, vol. 3, no. 1, pp. 101–110, Mar. 2015.



**Wei Zhang** (S'11) received the B.Sc. degree from Hefei University of Technology, Hefei, China, in 2007; the M.Sc. degree from Nanjing University of Aeronautics and Astronautics, Nanjing, China, in 2010; and the Ph.D. degree from the Hong Kong Polytechnic University, Kowloon, Hong Kong, in 2014, all in electrical engineering.

He is currently a Postdoctoral Fellow with the University of Michigan, Dearborn, MI, USA. His current research interests include wireless power transfer systems and resonant converters.



**Chunting Chris Mi** (S'00-A'01-M'01-SM'03-F'12) received the B.S.E.E degree in 1985, the M.S.E.E degree in 1988 from Northwestern Polytechnical University, Xi'an, China, and the Ph.D. degree in 2001 from the University of Toronto, Toronto, ON, Canada, all in electrical engineering.

He is a Professor and Chair of the Department of Electrical and Computer Engineering with San Diego State University, San Diego, CA, USA. He was an Electrical Engineer with General Electric Canada Inc., Toronto, ON, Canada. He was a Professor and the Director of the Department-of-Energy-funded Graduate Automotive Technology Education Center for Electric Drive Transportation with the University of Michigan, Dearborn, MI, USA. He has conducted extensive research and authored more than 100 articles. His current research interests include electric drives, power electronics, electric machines, renewable energy systems, and electric and hybrid vehicles.

Dr. Mi was the Chair from 2008 to 2009 and the Vice Chair from 2006 to 2007 of the IEEE Southeastern Michigan Section. He is an Area Editor of the IEEE TRANSACTIONS ON VEHICULAR TECHNOLOGY and the IEEE TRANSACTIONS ON POWER ELECTRONICS and an Associate Editor of the IEEE TRANSACTIONS ON INDUSTRY APPLICATIONS. He was a recipient of the Distinguished Teaching Award and the Distinguished Research Award of the University of Michigan, the 2007 IEEE Region 4 Outstanding Engineer Award, the IEEE Southeastern Michigan Section Outstanding Professional Award, and the SAE Environmental Excellence in Transportation Award.